A&A 663, L9 (2022)
https://doi.org/10.1051/0004-6361/202244399
© J. Cernicharo et al. 2022

Astronomy & Astrophysics

LETTER TO THE EDITOR

Discovery of fulvenallene in TMC-1 with the QUIJOTE line survey*

J. Cernicharo[1], R. Fuentetaja[1], M. Agúndez[1], R. I. Kaiser[2], C. Cabezas[1], N. Marcelino[3,4], B. Tercero[3,4], J. R. Pardo[1], and P. de Vicente[3]

[1] Grupo de Astrofísica Molecular, Instituto de Física Fundamental (IFF-CSIC), C/ Serrano 121, 28006 Madrid, Spain
e-mail: jose.cernicharo@csic.es
[2] Department of Chemistry, University of Hawaii at Manoa, Honolulu, HI 96822, USA
[3] Observatorio de Yebes, IGN, Cerro de la Palera s/n, 19141 Yebes, Guadalajara, Spain
[4] Observatorio Astronómico Nacional, IGN, C/Alfonso XII 3, 28014 Madrid, Spain

Received 1 July 2022 / Accepted 11 July 2022

ABSTRACT

We report the detection of fulvenallene (c-$C_5H_4CCH_2$) in the direction of TMC-1 with the QUIJOTE[1] line survey. Thirty rotational transitions with K_a = 0,1,2,3 and J = 9−15 were detected. The best rotational temperature fitting of the data is 9 K and a derived column density is $(2.7 \pm 0.3) \times 10^{12}$ cm^{-2}, which is only a factor of 4.4 below that of its potential precursor cyclopentadiene (c-C_5H_6), and 1.4–1.9 times higher than that of the ethynyl derivatives of cyclopentadiene. We searched for fulvene (c-$C_5H_4CH_2$), a CH_2 derivative of cyclopentadiene, for which we derive a 3σ upper limit to its column density of $(3.5 \pm 0.5) \times 10^{12}$ cm^{-2}. Upper limits were also obtained for toluene ($C_6H_5CH_3$) and styrene ($C_6H_5C_2H_3$), the methyl and vinyl derivatives of benzene. Fulvenallene and ethynyl cyclopentadiene are likely formed in the reaction between cyclopentadiene (c-C_5H_6) and the ehtynyl radical (CCH). However, the bottom-up gas-phase synthesis of cycles in TMC-1 underestimates the abundance of cyclopentadiene by two orders of magnitude, which strengthens the need to study all possible chemical pathways to cyclisation in cold dark cloud environments, such as TMC-1. However, the inclusion of the reaction between $C_3H_3^+$ and C_2H_4 produces a good agreement between model and observed abundances.

Key words. molecular data – line: identification – ISM: molecules – ISM: individual objects: TMC-1 – astrochemistry

1. Introduction

The QUIJOTE[1] line survey of TMC-1 (Cernicharo et al. 2021a) performed with the Yebes 40 m radio telescope has permitted the detection of nearly 40 new molecular species in recent months, most of which are hydrocarbons and cycles such as indene, benzyne, cyclopentadiene, and two isomers of ethynyl cyclopentadiene (see e.g., Cernicharo et al. 2021a,b,c,d,e and references therein). Propargyl (CH_2CCH) has been found to be one of the most abundant hydrocarbon radicals in this source (Agúndez et al. 2021, 2022). Other hydrocarbons such as ethynylallene ($CH_2CCHCCH$), vinylacetylene (CH_2CHCCH), and butadiynylallene (CH_2CCHC_4H) have also been found to have high abundances (Cernicharo et al. 2021b,d; Fuentetaja et al. 2022). Moreover, cyano derivatives of benzene and naphthalene have also been found towards TMC-1 (McGuire et al. 2018, 2021). This suggests that benzene and naphthalene are also very abundant in this cold prestellar core. To understand the formation of these species in the gas-phase, and their large abundances (see Appendix A), we have to consider very fast reactions between a few precursors. It is possible, however, that some gas-phase chemical reactions are still missing in the chemical networks. It is also likely that important hydrocarbons with low dipole moments are still awaiting detection. Hence, discovering new hydrocarbons through sensitive line surveys will certainly help in getting a complete chemical network (gas-phase and dust surface reactions) to explain the chemistry of hydrocarbons and polycyclic aromatic hydrocarbons (PAHs) in TMC-1.

In this Letter we report the discovery of fulvenallene (c-$C_5H_4CCH_2$) through the detection of 30 rotational transitions in the frequency range 31–50 GHz. The structure of fulvenallene (c-$C_5H_4CCH_2$), an isomer of ethynyl cyclopentadiene, is shown in Fig. 1. We discuss the chemistry of this hydrocarbon cycle in the context of a bottom-up gas-phase scheme for the formation of hydrocarbon cycles in TMC-1.

2. Observations

New receivers built within the Nanocosmos project[2], and installed at the Yebes 40m radiotelescope, were used for the observations of TMC-1 (α_{J2000} = 4^{h}41^{m}41.9^s and δ_{J2000} = +25°41′27.0″). A detailed description of the system is given by Tercero et al. (2021). Details of the QUIJOTE line survey are provided by Cernicharo et al. (2021a). The observations were carried out during different observing runs between November 2019 and May 2022. The receiver consists of two cold high electron mobility transistor amplifiers covering the 31.0–50.3 GHz band with horizontal and vertical polarisations. Receiver temperatures in the runs achieved during 2020 vary from 22 K

* Based on observations carried out with the Yebes 40m telescope (projects 19A003, 20A014, 20D023, and 21A011). The 40m radiotelescope at Yebes Observatory is operated by the Spanish Geographic Institute (IGN, Ministerio de Transportes, Movilidad y Agenda Urbana).
[1] Q-band Ultrasensitive Inspection Journey to the Obscure TMC-1 Environment

[2] https://nanocosmos.iff.csic.es/

Open Access article, published by EDP Sciences, under the terms of the Creative Commons Attribution License (https://creativecommons.org/licenses/by/4.0), which permits unrestricted use, distribution, and reproduction in any medium, provided the original work is properly cited.
This article is published in open access under the Subscribe-to-Open model. Subscribe to A&A to support open access publication.

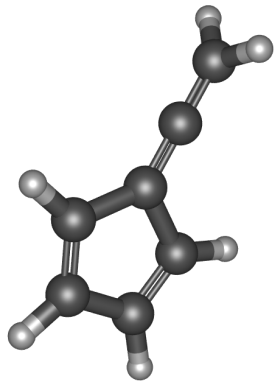

Fig. 1. Structure of fulvenallene (c-$C_5H_4CCH_2$).

at 32 GHz to 42 K at 50 GHz. Some power adaptation in the down-conversion chains reduced the receiver temperatures during 2021 to 16 K at 32 GHz and 25 K at 50 GHz. The backends are $2 \times 8 \times 2.5$ GHz fast Fourier transform spectrometers with a spectral resolution of 38.15 kHz providing the whole coverage of the Q band in each polarisation.

The data presented here correspond to 546 h of observing time on the source, of which 293 and 253 h were acquired with a frequency switching throw of 8 MHz and 10 MHz, respectively. The data analysis procedure is described in Appendix B. The intensity scale used in this work, antenna temperature (T_A^*), was calibrated using two absorbers at different temperatures and the atmospheric transmission model ATM (Cernicharo 1985; Pardo et al. 2001). The antenna temperature has an estimated uncertainty of 10% and can be converted to main beam brightness temperature, T_{mb}, by dividing by B_{eff}/F_{eff}. For the Yebes 40 m telescope, $B_{eff} = 0.738\ \exp[-(\nu(\mathrm{GHz})/72.2)^2]$ and $F_{eff} = 0.97$ (Tercero et al. 2021). All data were analysed using the GILDAS package[3].

3. Results

QUIJOTE has now reached a level of sensitivity (0.1–0.3 mK per 38.15 kHz channel across the Q band) that permits the detection of new isotopologues and derivatives of abundant species. Examples of detection and complete spectral characterisation of rare isotopologues through QUIJOTE data are HDCCN (Cabezas et al. 2021a), CH_2DC_3N (Cabezas et al. 2021b), and CH_2DC_4H (Cabezas et al. 2022a). Although QUIJOTE has not yet reached the confusion limit, special care should be taken when assigning lines to a given molecule as blending with other features often occurs. Line identification in this work was done using the following catalogues: MADEX (Cernicharo 2012), CDMS (Müller et al. 2005), and JPL (Pickett et al. 1998). By May 2022 the MADEX catalogue had 6434 spectral entries corresponding to the ground state and vibrationally excited state, together with the corresponding isotopologues, of 1734 molecules.

Rotational spectroscopy of fulvenallene was performed in the laboratory by Sakaizumi et al. (1993) up to frequencies of 39.3 GHz with an accuracy of 50 kHz, and by McCarthy et al. (2020) up to frequencies of 25 GHz with an accuracy of 2 kHz. To search for fulvanellene in TMC-1 we fitted these data, but discarded the less accurate measurements of Sakaizumi et al. (1993), which are also present in the data set of McCarthy et al. (2020). The derived rotational and distortion constants are shown in the middle column of Table 1, and were implemented in the MADEX code to predict the spectrum. Fulvenallene has C_{2v} symmetry, hence we have included the statistical weights for the ortho and para species, 9 for ortho (K_a odd) and 7 for para (K_a even). The energy difference between the two states is 0.47 K.

Table 1. Derived rotational constants for c-$C_5H_4CCH_2$.

Constant [a] (MHz)	TMC-1 [b]	Laboratory [c]	Merged fit [d]
A	8180.862(38)	8180.813(24)	8180.855(20)
B	1886.66733(64)	1886.67218(25)	1886.67152(19)
C	1549.11498(74)	1549.11344(26)	1549.11379(17)
$\Delta_J \times 10^5$	3.61(20)	4.46(15)	4.263(70)
$\Delta_{JK} \times 10^3$	3.007(70)	3.0085(70)	3.0065(77)
$\delta_J \times 10^5$		1.07(19)	0.602(60)
N_{lines} [e]	30	97	127
rms [f]	19	34	31
J_{max} [g]	15	11	15
$K_{a,max}$ [g]	3	10	10
ν_{max} [h]	48 420.601	39 354.900	48 420.601

Notes. [a]Fitted rotational and distortion constants. The values in brackets correspond to the uncertainties of the parameters in units of the last significant digits. [b]Fit to the line frequencies observed in TMC-1 alone. [c]Fit to the laboratory data (see text). [d]Merged fit to the laboratory and TMC-1 data (see Table C.1). [e]Number of lines in the fit. [f]The standard deviation of the fit in kHz. [g]Maximum value of J and K_a of the lines included in the fit. [h]Maximum frequency of the lines included in the fit in MHz.

We first searched for the strongest lines, which correspond to transitions with $K_a = 0$ and 1. All $K_a = 0{,}1$ lines within the Q band corresponding to transitions with J between 9 and 14 (a total of sixteen lines) are detected. These lines were found within 10–20 kHz of the predicted frequencies and are shown in Fig. 2. Their line parameters are given in Table C.1. Once the $K_a = 0$ and 1 lines were detected we searched for the less intense $K_a = 2$ and 3 transitions. Fourteen of these lines were detected and are shown in Fig. 3; their line parameters are given in Table C.1. We note that two of these lines are shown in Fig. 2 in the upper left panel and the fourth panel from the bottom on the right. Although the differences between the observed and predicted frequencies are small, they show a systematic behaviour; in particular, some of the $K_a = 2{,}3$ lines show discrepancies with respect to their frequencies as large as 50 kHz. Taking into account that the predictions in the Q band are strongly dependent on the low accuracy data of Sakaizumi et al. (1993) we fitted the frequencies of the TMC-1 lines alone to a Watson Hamiltonian in reduction A representation I^r (Watson et al. 1977) using the FITWAT code (Cernicharo et al. 2018). This code reproduces the same results as the standard SPFIT code of Pickett (1991), as detailed in Appendix A of Cernicharo et al. (2018). The frequency measurements have been weighted as $1/\sigma^2$, where σ is the estimated frequency uncertainty. The resulting parameters are given in the first column of Table 1. The comparison with the fit to the laboratory data (middle column of the same table) indicates that all the observed lines can be reproduced with rotational and distortion constants identical to those of the laboratory within the derived uncertainties of the different constants. Hence, the detection of fulvenallene is solid as it is based on 30 individual lines. Finally, taking into account that the accuracy of our measurements in the 31–50 GHz domain is better than those of Sakaizumi et al. (1993), we performed a merged

[3] http://www.iram.fr/IRAMFR/GILDAS

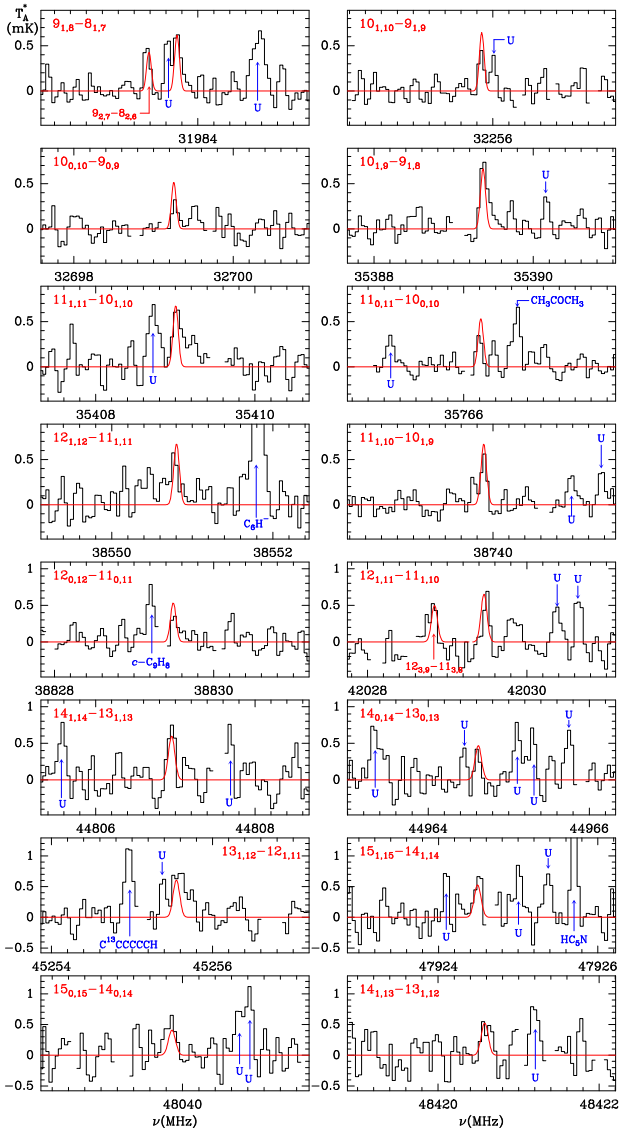

Fig. 2. Observed lines with K_a = 0,1 of fulvenallene(c-$C_5H_4CCH_2$) towards TMC-1 (see line parameters in Table C.1). The abscissa corresponds to the rest frequency assuming a local standard of rest velocity of 5.83 km s^{-1}. The ordinate is the antenna temperature corrected for atmospheric and telescope losses in mK. The red line shows the synthetic spectrum derived for $T_{\rm rot}$ = 10 K and N(c-$C_5H_4CCH_2$) = 2.7×10^{12} cm^{-2}. Blank channels correspond to negative features produced in the folding of the frequency switching data. Some K_a = 2,3 lines also appear in these panels (*top left and fourth from bottom right*). Additional K_a = 2,3 lines are shown in Fig. 3.

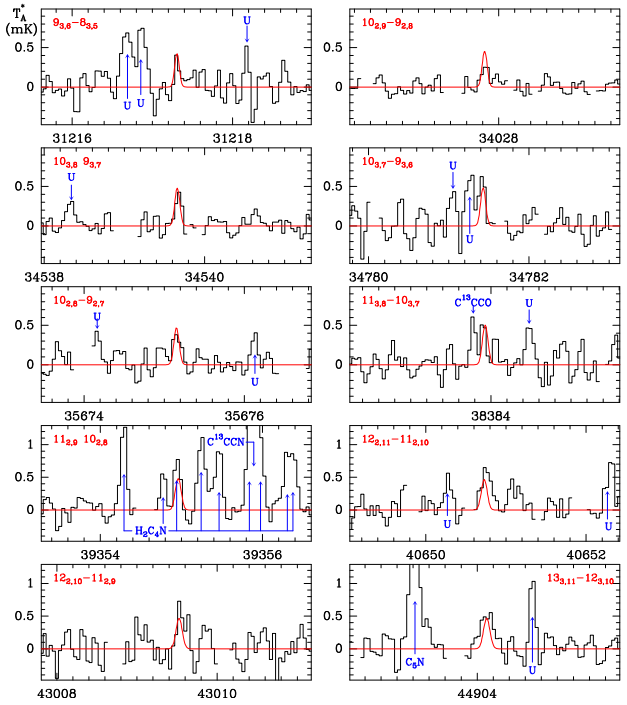

Fig. 3. Same as in Fig. 1, but for lines K_a = 2 and 3 (see line parameters in Table C.1).

fit to the laboratory and space frequencies of fulvenallene. The resulting constants are given in the third column of Table 1 and represent a significant improvement with respect to the constants obtained from the laboratory data alone (middle column of Table 1). The constants resulting from this merged fit are the ones we recommend to predict the spectrum of fulvenallene. The observed and calculated frequencies of the lines included in the fit, and the difference between the observed and calculated frequencies are given in Table C.2.

Once we are confident of the detection of fulvenallene in TMC-1, we fitted the observed lines using a line profile fit method (Cernicharo et al. 2021e), which permits the rotational temperature and the column density to be fit, assuming that all levels have the same rotational temperature. A value of the dipole moment μ_a = 0.69 ± 0.10 D was used (Sakaizumi et al. 1993). We obtained a rotational temperature of 9 ± 1 K and a column density of $(2.7\pm0.3)\times10^{12}$ cm^{-2}. A rotational temperature lower than 8 K cannot reproduce the observed intensities of the K_a = 2,3 lines.

We also searched for fulvene (c-$C_5H_4CH_2$), for which the rotational spectroscopy has been accurately recorded by McCarthy et al. (2020). The dipole moment of this molecule is μ_a = 0.424±0.001 D (Baron et al. 1972), and hence for a column density similar to that of fulvenallene the lines will be 2.6 times weaker. Although some K_a = 0,1 lines are detected at a 3σ level we conclude that the molecule is below the present sensitivity limit of QUIJOTE. We obtain a 3σ upper limit to the column density of 3.5×10^{12} cm^{-2} for fulvene.

Two derivatives of benzene are also of interest in the context of this work, toluene (c-$C_6H_5CH_3$) and styrene (c-$C_6H_5C_2H_3$). For toluene, we used the laboratory data of Kisiel et al. (2004) and the dipole moment obtained by Rudolph et al. (1967), μ_a = 0.38 ± 0.01 D. For styrene, laboratory spectroscopy up to 18 GHz is available from Caminati et al. (1988), who also derived the a and b components of the dipole moment as μ_a = 0.122 ± 0.001 D and μ_b<0.02 D. Due to the low dipole moment of the two species we derived relatively high 3σ upper limits, 6×10^{12} cm^{-2} for toluene and 10^{14} cm^{-2} for styrene. For both species we adopted a rotational temperature of 9 K.

4. Discussion

In the frame of a gas-phase bottom-up scenario for the formation of cycles in TMC-1, we ran chemical model calculations similar to those presented in Cernicharo et al. (2021f). Here we focus on cyclopentadiene and derivatives. Cyclopentadiene can be formed by two successive reactions involving the radical CH

$$CH_3CHCH_2 + CH \rightarrow CH_2CHCHCH_2 + H, \quad (1)$$

$$CH_2CHCHCH_2 + CH \rightarrow c - C_5H_6 + H, \quad (2)$$

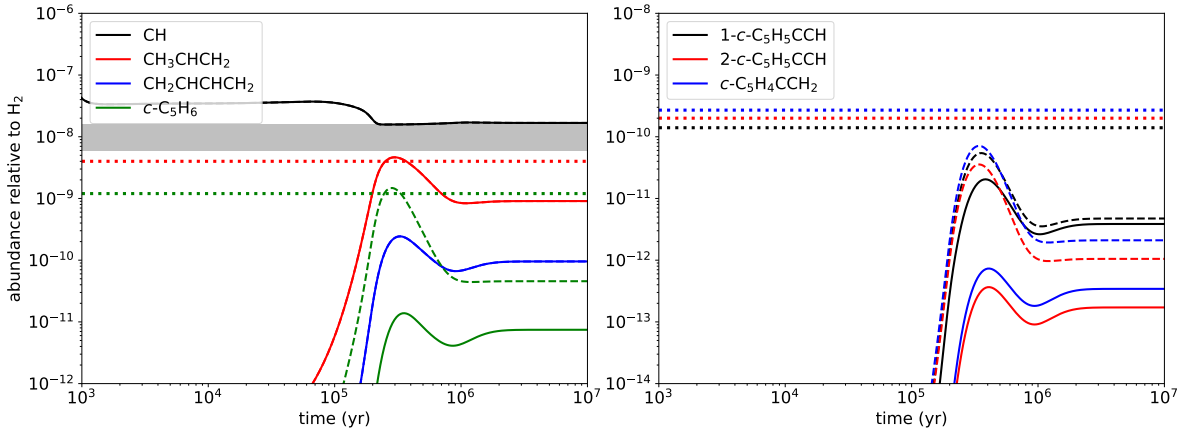

Fig. 4. Calculated abundances for c-C_5H_6 and its precursors (*left panel*) and for the products of its reaction with CCH (*right panel*). Solid lines correspond to the standard chemical model, while dashed lines correspond to a model including formation of c-C_5H_6 involving the reaction l-$C_3H_3^+$ + C_2H_4 (see text). The horizontal band and dotted lines correspond to the abundances observed in TMC-1 (see Table A.1).

for which we adopted rate coefficients at 10 K of 3.3×10^{-10} cm^3 s^{-1} (Loison et al. 2017) and 4×10^{-10} cm^3 s^{-1} (Cernicharo et al. 2021f), respectively. In turn, the reaction of c-C_5H_6 with CCH can yield various isomers of ethynyl cyclopentadiene, as well as fulvenallene

$$\mathrm{c-C_5H_6 + CCH \rightarrow 1-c-C_5H_5CCH + H}, \quad (3a)$$
$$\rightarrow \mathrm{2-c-C_5H_5CCH + H}, \quad (3b)$$
$$\rightarrow \mathrm{c-C_5H_4CCH_2 + H}. \quad (3c)$$

We assumed a rate coefficient of 4×10^{-10} cm^3 s^{-1} for reaction (3) and branching ratios of 0.25, 0.25, and 0.50 for channels (3a), (3b), and (3c), respectively, where a higher branching ratio is adopted for fulvenallene because it is more stable than the isomers of ethynyl cyclopentadiene.

The synthesis of c-C_5H_6 therefore relies on 1,3-butadiene ($CH_2CHCHCH_2$; non-polar and thus invisible at radio wavelengths), which in turn is formed from propene (CH_2CHCH_3), whose abundance is well constrained in TMC-1 (Marcelino et al. 2007). In the chemical model presented in Cernicharo et al. (2021f) this pathway produced cyclopentadiene with an abundance in agreement with observations because propene was formed very efficiently due to two consecutive radiative associations of CH_2CCH^+ with H_2 (Herbst et al. 2010), followed by dissociative recombination of $C_3H_7^+$. This pathway is included in the chemical networks UMIST RATE12 (McElroy et al. 2013) and `kida.uva.2014` (Wakelam et al. 2015) and yields a very high propene abundance (see e.g., Agúndez & Wakelam 2013). However, the radiative associations mentioned above were later on shown to be inefficient at low temperatures (Lin et al. 2013). If they are neglected, the calculated abundance of propene drops by many orders of magnitude, well below the observed value, with drastic implications for the chemistry of many other hydrocarbons, such as 1,3-butadiene and cyclopentadiene, which are direct descendants of propene.

Currently, no efficient gas-phase route to propene has been identified in cold dark clouds. However, we know from observations that propene is present with a fairly large abundance. To overcome the lack of formation of propene in our gas-phase chemical model, we fixed the peak abundance of propene to be in agreement with the value observed in TMC-1. The results from the chemical model are shown as solid lines in Fig. 4. It is seen that 1,3-butadiene is formed with an abundance ten times lower than propene, while c-C_5H_6 in turn reaches an abundance ten times below that of 1,3-butadiene. However, according to the observations, the abundance of c-C_5H_6 is only slightly below that of propene. The chemical model thus underestimates the abundance of c-C_5H_6 by two orders of magnitude, and this translates directly to the derivatives of cyclopentadiene resulting from its reaction with CCH. In the case of 1-c-C_5H_5CCH, its calculated abundance is higher than that of 2-c-C_5H_5CCH and fuvenallene because it is formed through reaction (3), and in addition by the reaction between C_3H and 1,3-butadiene (see Cernicharo et al. 2021e).

The fact that 1,3-butadiene and cyclopentadiene are first- and second-generation descendants of propene means that they reach progressively lower abundances. The resulting abundances are essentially controlled by the rates of formation, through reactions (1) and (2), and the rates of destruction, which in the chemical model is dominated by reaction with atomic carbon. We assumed rate coefficients of 10^{-10} cm^3 s^{-1} for the reactions of atomic carbon with 1,3-butadiene and cyclopentadiene, in line with the values determined experimentally at low temperature for reactions between C and unsaturated hydrocarbons (Chastaing et al. 2001). In summary, regardless of what the true pathway to propene is, the consecutive reactions with CH are found to be insufficient to form cyclopentadiene with the observed abundance.

We examined possible formation routes to c-C_5H_6 involving cations. Among them, the reaction between l-$C_3H_3^+$ and C_2H_4 has been measured to be rapid, with a rate coefficient of 1.1×10^{-9} cm^3 s^{-1}, and the ion $C_5H_7^+$ has been observed as product (Smyth et al. 1982; Anicich 2003). Including this reaction in the chemical model and assuming that the ion $C_5H_7^+$ is cyclic and recombines dissociatively with electrons to yield c-C_5H_6 with a standard rate coefficient of 10^{-7} $(T/300)^{-0.5}$ cm^3 s^{-1}, the calculated peak abundances of cyclopentadiene, and those of its CCH derivatives c-C_5H_5CCH and c-$C_5H_4CCH_2$, become close to the observed values (see dashed lines in Fig. 4). Although our assumptions on the l-$C_3H_3^+ + C_2H_4$ reaction require further experimental or theoretical support, this suggests that ion-neutral reactions can provide efficient formation routes to cycles in TMC-1. We note that c-$C_3H_3^+$ does not react with C_2H_4 (Smyth et al. 1982; Anicich 2003).

To have some insight into the possible precursors of hydrocarbon cycles we collected abundances for hydrocarbons C_nH_m detected in TMC-1. The abundances derived from QUIJOTE data from previous publications of our team related to newly

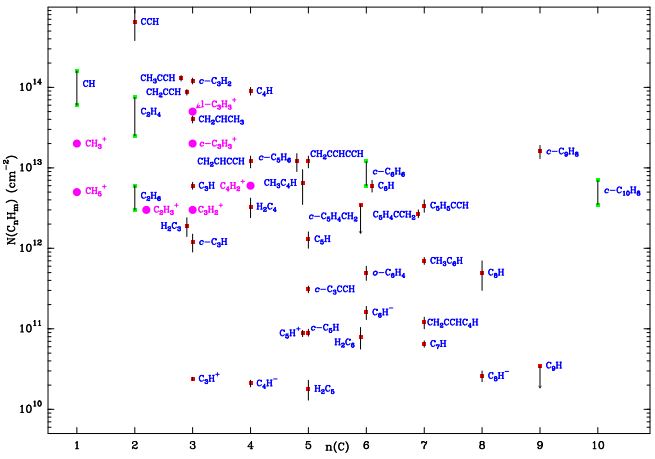

Fig. 5. Graphic representation of the abundances of C_nH_m hydrocarbons from Table A.1. The abscissa corresponds to the number of carbon atoms in the molecule and the ordinate to the column density of each hydrocarbon. For species whose abundance has been estimated from cyano derivatives the upper and lower ranges are indicated by two green squares. For the other species the abundance is indicated by a single red square and the error is represented by a vertical black line. Abundances of the most abundant cations, according to the chemical model (see text), are indicated in magenta.

detected hydrocarbons, and for species already known but with transitions in our frequency range, are given in Table A.1 and represented in Fig. 5. For species such as benzene or naphthalene we adopted an abundance ratio between them and their cyano derivatives of 5–10. We note however that these estimates are very uncertain. From Fig. 5 it appears that the most abundant hydrocarbon radicals are methylidyne (CH), ethynyl (CCH), propargyl (CH_2CCH), and butadiynyl (C_4H). The most abundant closed shell hydrocarbons are methylacetylene (CH_3CCH), cyclopropenylidyne (c-C_3H_2), ethylene (C_2H_4), and propene (CH_2CHCH_3). Indene is the most abundant cycle with more than three carbon atoms, followed by cyclopentadiene, benzene, naphthalene, and benzyne. If these rings are formed in the gas phase, their precursors should be among the abundant species with 3–5 carbon atoms. The role of hydrocarbon cations ($C_nH_m^+$) in the chemistry of hydrocarbons has been quite well studied, but their abundances remain unknown. Only C_3H^+ and C_5H^+ have been detected in TMC-1 so far (Cernicharo et al. 2022). Moreover, the abundance of important species for hydrocarbon chemistry, such as CH_3, CH_4, C_2H_2, CH_2CH_2, CH_3CH_3, and $CH_3CH_2CH_3$, remain unknown because they are non-polar, and thus cannot be observed at radio wavelengths. For CH_2CH_2 we used the derived abundance of vinyl acetylene (see Appendix A) since molecular beam experiments and electronic structure calculations provide compelling evidence that it is formed in the reaction of ethylene and the ethynyl radical (Zhang et al. 2009). Similarly, for CH_3CH_3 we can estimate its abundance from that of CH_3CH_2CCH (Cernicharo et al. 2021d). These estimates are, as for benzene and naphthalene, very uncertain (see Appendix A).

5. Conclusions

We detected fulvenallene in TMC-1, with an abundance just 4.4 times lower than its possible precursor cyclopentadiene and similar to those of the two ethynyl cyclopentadiene isomers detected in this source. Fulvenallene and ethynyl cyclopentadiene are most likely formed by the reaction between cyclopentadiene and CCH. However, our chemical model, mainly based on neutral-neutral gas-phase reactions, undererstimates the abundance of cyclopentadiene by two orders of magnitude. We suggest that ion-neutral gas-phase reactions between the most abundant cations and hydrocarbons, open and closed shell species, may provide efficient routes to cyclopentadiene and other cycles in TMC-1.

Acknowledgements. We thank ERC for funding through grant ERC-2013-Syg-610256-NANOCOSMOS. We also thank Ministerio de Ciencia e Innovación of Spain (MICIU) for funding support through projects PID2019-106110GB-I00, PID2019-107115GB-C21, and PID2019-106235GB-I00.

References

Agúndez, M., & Wakelam, V. 2013, Chem. Rev., 113, 8710
Agúndez, M., Cabezas, C., Tercero, B., et al. 2021, A&A, 647, L10
Agúndez, M., Marcelino, N., Cabezas, C., et al. 2022, A&A, 657, A96
Anicich, V. G. 2003, JPL Publication 03–19
Baron, P. A., Brown, R. D., Burden, F. R., et al. 1972, J. Mol. Spectrosc., 43, 401
Cabezas, C., Endo, Y., Roueff, E., et al. 2021a, A&A, 646, L1
Cabezas, C., Roueff, E., Tercero, B., et al. 2021b, A&A, 650, L15
Cabezas, C., Tercero, B., Agúndez, M., et al. 2021c, A&A, 650, L9
Cabezas, C., Fuentetaja, R., Roueff, E., et al. 2022a, A&A, 657, L5
Cabezas, C., Agúndez, M., Fuentetaja, R., et al. 2022b, A&A, 663, L2
Caminati, W., Volgelsanger, B., & Bauder, A. 1988, J. Mol. Spectrosc., 128, 384
Cernicharo, J. 1985, Internal IRAM report (Granada: IRAM)
Cernicharo, J. 2012, in ECLA 2011: Proc. of the European Conference on Laboratory Astrophysics, eds. C. Stehl, C. Joblin, & L. d'Hendecourt (Cambridge: Cambridge Univ. Press), EAS Publ. Ser., 251
Cernicharo, J., & Guélin, M. 1987, A&A, 176, 299
Cernicharo, J., Guélin, M., Agúndez, M., et al. 2018, A&A, 618, A4
Cernicharo, J., Agúndez, M., Kaiser, R., et al. 2021a, A&A, 652, L9
Cernicharo, J., Cabezas, C., Agúndez, M., et al. 2021b, A&A, 647, L3
Cernicharo, J., Agúndez, M., Cabezas, C., et al. 2021c, A&A, 649, L15
Cernicharo, J., Agúndez, M., Cabezas, C., et al. 2021d, A&A, 647, L2
Cernicharo, J., Agúndez, M., Kaiser, R. I., et al. 2021e, A&A, 655, L1
Cernicharo, J., Cabezas, C., Agúndez, M., et al. 2021f, A&A, 648, L3
Cernicharo, J., Cabezas, C., Endo, Y., et al. 2021g, A&A, 646, L3
Cernicharo, J., Agúndez, M., Cabezas, C., et al. 2022, A&A, 657, L6
Chastaing, D., Le Picard, S. D., Sims, I. R., & Smith, I. W. M. 2001, A&A, 365, 241
Fossé, D., Cernicharo, J., Gerin, M., & Cox, P. 2001, ApJ, 552, 168
Fuentetaja, R., Cabezas, C., Agúndez, M., et al. 2022, A&A, 663, L3
Herbst, E., Roueff, E., & Talbi, D. 2010, Mol. Phys., 108, 2171
Hjalmarson, A., Sume, A., Elldér, J., et al. 1977, ApJS, 35, 263
Kaifu, N., Ohishi, M., Kawaguchi, K., et al. 2004, PASJ, 56, 69
Kisiel, Z., Bialkowska-Jaworska, E., Pszczólkowski, L., & Mäder, H. 2004, J. Mol. Spectrosc., 227, 109
Lin, Z., Talbi, D., Roueff, E., et al. 2013, ApJ, 765, 80
Loison, J.-C., Agúndez, M., Wakelam, V., et al. 2017, MNRAS, 470, 4075
Marcelino, N., Cernicharo, J., Agúndez, M., et al. 2007, ApJ, 665, L127
McCarthy, M. C., Lee, K. L. K., Carroll, P. B., et al. 2020, J. Phys. Chem. A, 124, 5170
McElroy, D., Walsh, C., Markwick, A. J., et al. 2013, A&A, 550, A36
McGuire, B. A., Burkhardt, A. M., Kalenskii, S., et al. 2018, Science, 359, 202
McGuire, B. A., Loomis, R. A., Burkhardt, A. M., et al. 2021, Science, 371, 1265
Müller, H. S. P., Schlöder, F., Stutzki, J., & Winnewisser, G. 2005, J. Mol. Struct., 742, 215
Pardo, J. R., Cernicharo, J., & Serabyn, E. 2001, IEEE Trans. Antennas and Propagation, 49, 12
Pickett, H. M. 1991, J. Mol. Spectrosc., 148, 371
Pickett, H. M., Poynter, R. L., Cohen, E. A., et al. 1998, J. Quant. Spectrosc. Radiat. Transfer, 60, 883
Rudolph, H. D., Jaeschke, A., & Wendling, P. 1967, Z. Naturforschg., 22a, 940
Sakai, N., Saruwatari, O., Sakai, T., et al. 2010, A&A, 512, A31
Sakaizumi, T., Katoh, F., Ohashi, O., & Yamaguchi, I. 1993, J. Mol. Spectrosc., 159, 112
Smyth, K. C., Lias, S. G., & Ausloos, P. 1982, Combust. Sci. Technol., 28, 147
Tercero, F., López-Pérez, J. A., Gallego, J. D., et al. 2021, A&A, 645, A37
Wakelam, V., Loison, J.-C., Herbst, E., et al. 2015, ApJS, 217, 20
Watson, J. K. G. 1977, ed. J. Durig Vibration Spectra and Structure (Amsterdam: Elsevier), 6, 1
Zhang, F., Kim, S., Kaiser, R. I., et al. 2009, J. Phys. Chem. A, 113, 11167

Appendix A: Abundance of the C_nH_m hydrocarbons in TMC-1

In order to have a global view of the abundances of hydrocarbons in TMC-1, we show in Table A.1 the values obtained with QUIJOTE for most species of interest related to this work. In all cases we assumed a source diameter of 80″ (Fossé et al. 2001). Some of the species given in this table have rotational transitions within the QUIJOTE survey, but their data have not been published yet. Most of them have been previously detected by other authors. Nevertheless, we think it more valuable to provide column densities using the QUIJOTE data to have a coherent criteria in the determination of their column densities, and to use data gathered with the same radio telescope. The data on these species will be published elsewhere. Here we comment briefly on the assumptions adopted for these molecules to derive the column densities given in Table A.1. In all cases, except when indicated, the adopted line width at half intensity, Δv, is 0.6 km s^{-1}.

Table A.1. Column density of C_nH_m, C_nH^+, and C_nH^- species in TMC-1

Molecule	N (cm^{-2})	Abundance[a]	Ref.
CH	(6-16)×10^{13}	(6-16)×10^{-09}	1
CCH	(6.5±2.7)×10^{14}	(6.5±2.7)×10^{-08}	2
C_2H_4	(3-7)×10^{13}	(3-7)×10^{-09}	3a
CH_3CH_3	(3-6)×10^{12}	(3-6)×10^{-10}	3b
C_3H	(6.0±0.6)×10^{12}	(6.0±0.6)×10^{-10}	4
c-C_3H	(1.2±0.3)×10^{12}	(1.2±0.3)×10^{-10}	4
C_3H^+	(2.4±0.2)×10^{10}	(2.4±0.2)×10^{-12}	5
c−C_3H_2	(1.2±0.1)×10^{14}	(1.2±0.1)×10^{-08}	6
H_2C_3	(1.9±0.5)×10^{12}	(1.9±0.5)×10^{-10}	7
CH_2CCH	(8.7±0.7)×10^{13}	(8.7±0.7)×10^{-09}	8
CH_3CCH	(1.3±0.1)×10^{14}	(1.3±0.1)×10^{-08}	6
CH_2CHCH_3	(4.0±0.4)×10^{13}	(4.0±0.4)×10^{-09}	9
C_4H	(9.0±1.0)×10^{13}	(9.9±1.0)×10^{-09}	10
C_4H^-	(2.1±0.2)×10^{10}	(2.1±0.2)×10^{-12}	10
H_2C_4	(3.3±0.9)×10^{12}	(1.3±0.1)×10^{-10}	7
CH_2CHCCH	(1.2±0.2)×10^{13}	(1.2±0.2)×10^{-09}	11
C_5H	(1.3±0.3)×10^{12}	(1.3±0.3)×10^{-10}	12
c-C_5H	(9.0±0.9)×10^{10}	(9.0±0.9)×10^{-12}	12
C_5H^+	(8.8±0.5)×10^{10}	(8.8±0.5)×10^{-12}	5
c-C_3HCCH	(3.1±0.8)×10^{11}	(3.1±0.8)×10^{-11}	13
H_2C_5	(1.8±0.5)×10^{10}	(1.8±0.5)×10^{-12}	7
$CH_2CCHCCH$	(1.2±0.2)×10^{13}	(1.2±0.2)×10^{-09}	14
CH_3C_4H	(6.5±0.3)×10^{12}	(6.5±0.3)×10^{-10}	14
c-C_5H_6	(1.2±0.3)×10^{13}	(1.2±0.3)×10^{-09}	13
C_6H	(6.0±1.0)×10^{12}	(6.0±1.0)×10^{-10}	10
C_6H^-	(1.6±0.3)×10^{11}	(1.6±0.3)×10^{-11}	10
H_2C_6	(8.0±2.4)×10^{10}	(8.0±2.4)×10^{-12}	7
o-C_6H_4	(5.0±1.0)×10^{11}	(5.0±1.0)×10^{-11}	15
c-C_6H_6	(0.6-1.2)×10^{13}	(0.6-1.2)×10^{-09}	16
c-$C_5H_4CH_2$	≤3.5×10^{12}	≤3.5×10^{-10}	17
C_7H	(6.5±0.6)×10^{10}	(6.5±0.6)×10^{-12}	4
CH_2CCHC_4H	(1.2±0.2)×10^{11}	(1.2±0.2)×10^{-11}	18
CH_3C_6H	(7.0±0.7)×10^{11}	(7.0±0.7)×10^{-11}	18
1-*c*-C_5H_5CCH	(1.4±0.2)×10^{12}	(1.4±0.2)×10^{-10}	19
2-*c*-C_5H_5CCH	(2.0±0.4)×10^{12}	(2.0±0.2)×10^{-10}	19
***c*-$C_5H_4CCH_2$**	(2.7±0.3)×10^{12}	(2.7±0.3)×10^{-10}	17
c-$C_6H_5CH_3$	≤6.0×10^{12}	≤6.0×10^{-10}	17
C_8H	(5.0±2.1)×10^{11}	(5.0±2.1)×10^{-11}	10
C_8H^-	(2.6±0.4)×10^{10}	(2.6±0.4)×10^{-12}	10
c-$C_6H_5CHCH_2$	≤1.0×10^{14}	≤1.0×10^{-08}	17
C_9H	≤3.5×10^{10}	≤3.5×10^{-12}	4
c-C_9H_8	(1.6±0.3)×10^{13}	(1.6±0.3)×10^{-09}	13
1-*c*-$C_{10}H_8$	(3.5-7)×10^{12}	(3.5-7)×10^{-10}	20
2-*c*-$C_{10}H_8$	(3.5-7)×10^{12}	(3.5-7)×10^{-10}	20

Notes. [a]Assuming a H_2 column density of 10^{22} cm^{-2} (Cernicharo & Guélin 1987). [1]Range of column densities derived by Hjalmarson et al. (1977) towards several positions in Taurus, some of them around TMC-1. The quoted column densities of CH are representative of the Taurus complex. [2]Sakai et al. (2010). [3a]Estimated from the column density of CH_2CHCCH obtained by Cernicharo et al. (2021d) and assuming an abundance ratio between C_2H_4 and CH_2CHCCH ~3–6. [3b]Estimated from the column density of CH_3CH_2CCH obtained by Cernicharo et al. (2021d) and assuming an abundance ratio between C_2H_6 and CH_3CH_2CCH ~3–6. [4]See Appendix A [5]Cernicharo et al. (2022). [6]Cabezas et al. (2021a). [7]Cabezas et al. (2021c). [8]Agúndez et al. (2021). [9]Marcelino et al. (2007). [10]Agúndez et al., in preparation. [11]Cernicharo et al. (2021d). [12]Cabezas et al. (2022b). [13]Cernicharo et al. (2021c). [14]Cernicharo et al. (2021b). [15]Cernicharo et al. (2021a). [16]Estimated from the column density of C_6H_5CN obtained by Cernicharo et al. (2021f) and assuming an abundance ratio between benzene and benzonitrile ~5–10. [17]This work. [18]Fuentetaja et al. (2022). [19]Cernicharo et al. (2021f). [20]From the column density of the isomers of cyanonaphthalene derived by McGuire et al. (2021) assuming an abundance ratio of 5–10 between naphthalene and its cyano derivatives.

For *l*-C_3H, only one rotational transition, J=3/2-1/2, with six fine and hyperfine components is covered within the QUIJOTE frequency range. All these lines are detected with very high S/N values. We adopted T_{rot}=7 K for linear C_3H. The derived column density is (6.0±0.6)×10^{12} cm^{-2}. We note that the column density is not very sensitive to the adopted rotational temperature for T_{rot} between 6 and 10 K. This is due to the low energy (E_u=1.57 K) of the upper level J=3/2 (see Appendix A of Cernicharo et al. 2021g).

Only the rotational transition 2_{11}-2_{12} of *c*-C_3H falls within the QUIJOTE survey. It exhibits several fine and hyperfine components. The energy or the upper level of 6.52 K, hence slightly more sensitive to the adopted rotational temperature than C_3H. The derived column density is (1.2±0.3)×10^{12} cm^{-2} for T_{rot}=5 K and (9.0±0.9)×10^{11} cm^{-2} for T_{rot}=7 K.

For the hydrocarbon anions C_4H^-, C_6H^-, and C_8H^-, and for their neutral counterparts C_4H, C_6H, and C_8H, column densities were derived from all data available in the literature plus the QUIJOTE data. For these species, we derived column densities using both the LVG method and the rotation diagram method. In Table A.1 we give values of their column densities, where the uncertainty corresponds to the values derived from these two methods. More details will be given in a separate publication (Agúndez et al., in preparation).

Several transitions of C_7H are present within the survey. Their intensities are well reproduced with T_{rot}=7 K and a column density of (6.5±0.6)×10^{10} cm^{-2}. For C_9H we derived only

a 3σ upper limit of 3.5×10^{10} cm^{-2} adopting a rotational temperature of 10 K.

Several hydrocarbons of interest for this work have a zero dipole moment, and hence their abundances were estimated from their CCH or CN derivatives. We assumed an abundance ratio between the mother molecule and its cyano derivatives (benzene and naphthalene) of 5–10. In the case of ethynyl derivatives (C_2H_4, C_2H_6) the adopted abundance ratio is 3–6; however, these estimates are very uncertain.

Appendix B: Data analysis

The raw data of the QUIJOTE survey was processed always following the same procedure for each observing run, which typically consist of 100–120 h of observing time on the source. Each FFT spectrometer was divided into 160 subsections of 400 channels. Ripples with frequencies ≤5 MHz can be easily removed with the FFT command of the CLASS program of the GILDAS package. For each sub-band of 400 channels, a comparison of the sum of the raw data (averaged weighting by system temperature and integration time), the data with ripples was removed, and the results of the previous runs was performed to define line windows around features with intensity above 4σ, and also to remove instrumental spurious features, atmospheric lines, and well-known features arising in the down-conversion chain. Once this process was achieved, then all raw scans of a given run were processed removing a polynomial baseline. Taking into account that the lines have a width of 2–3 channels at half intensity, this baseline removal does not affect the line profiles. Once the baselines for all the scans of each 400-channel sub-band were removed, the data were averaged, but this time with weights proportional to $1/\sigma^2$. Because each run consists typically of 1000–2000 individual scans this procedure gives little statistical weight to scans that have a greater noise value than expected without having to explore all the individual scans. This rather tedious procedure yields flat baselines and full confidence in the spectral purity. A total of 2560 blocks of 400 channels have been analysed for each observing run (160× 8 spectrometers × two polarisations). Except for the first run for which the information used on the lines appearing in TMC-1 was that provided by the Nobeyama line survey of TMC-1 (Kaifu et al. 2004), for all the other runs QUIJOTE itself was the source of information on the spectral features present in each 400-channel sub-band. The final spectrum contains 507017 channels with a width of 38.15 kHz.

Appendix C: Line parameters

The line parameters in this work were obtained by fitting a Gaussian line profile to the observed data. A window of ± 15 km s^{-1} around the v_{LSR} of the source (5.83 km s^{-1}) was considered for each transition. The derived line parameters for fulvenallene are given in Table C.1. As indicated in Sect. 3, a merged fit of the derived frequencies in TMC-1 with the laboratory measurements of Sakaizumi et al. (1993) and McCarthy et al. (2020) was performed to improve the rotational and distortion constants. The list of lines, observed and calculated frequencies, and the difference between observed and calculated values are given in Table C.2. The recommended rotational and distortion constants are given in Table 1.

Table C.1. Observed line parameters for fulvanallene (c-$C_5H_4CCH_2$) in TMC-1

Transition	ν^a_{obs} (MHz)	$\int T_A^* dv$ ^{b} (mK km s^{-1})	Δv^c (km s^{-1})	T_A^* (mK)	N
$9_{3,6} - 8_{3,5}$	31217.308±0.020	0.24±0.10	0.51±0.41	0.45±0.16	
$9_{2,7} - 8_{2,6}$	31983.358±0.015	0.43±0.08	0.75±0.14	0.53±0.10	
$9_{1,8} - 8_{1,7}$	31983.739±0.010	0.78±0.13	1.16±0.24	0.63±0.10	
$10_{1,10} - 9_{1,9}$	32255.854±0.010	0.36±0.08	0.73±0.17	0.46±0.10	
$10_{0,10} - 9_{0,9}$	32699.259±0.015	0.27±0.08	0.82±0.31	0.31±0.10	
$10_{2,9} - 9_{2,8}$	34027.832±0.015	0.28±0.06	0.92±0.24	0.28±0.09	
$10_{3,8} - 9_{3,7}$	34539.679±0.010	0.34±0.07	0.72±0.16	0.45±0.10	
$10_{3,7} - 9_{3,6}$	34781.417±0.010	0.51±0.12	0.71±0.18	0.67±0.15	A
$10_{1,9} - 9_{1,8}$	35389.366±0.010	0.50±0.09	0.69±0.14	0.68±0.10	
$11_{1,11} - 10_{1,10}$	35409.019±0.010	0.59±0.06	0.97±0.24	0.58±0.14	B
$10_{2,8} - 9_{2,7}$	35675.155±0.015	0.42±0.10	1.02±0.40	0.39±0.12	
$11_{0,11} - 10_{0,10}$	35766.192±0.015	0.24±0.05	0.62±0.11	0.36±0.09	
$11_{2,10} - 10_{2,9}$	37349.808±0.015	0.37±0.07	0.75±0.15	0.46±0.12	A
$11_{3,9} - 10_{3,8}$	38002.363±0.020	0.10±0.04	0.41±0.14	0.23±0.09	
$11_{3,8} - 10_{3,7}$	38383.903±0.020	0.35±0.09	0.55±0.21	0.60±0.14	B
$12_{1,12} - 11_{1,11}$	38550.784±0.015	0.23±0.07	0.66±0.26	0.44±0.13	B
$11_{1,10} - 10_{1,9}$	38739.886±0.010	0.37±0.05	0.60±0.09	0.58±0.09	
$12_{0,12} - 11_{0,11}$	38829.515±0.015	0.29±0.10	0.79±0.42	0.35±0.11	
$11_{2,9} - 10_{2,8}$	39354.949±0.030	0.57±0.05	0.65±0.08	0.83±0.13	C
$12_{2,11} - 11_{2,10}$	40650.743±0.020	0.42±0.49	1.09±0.80	0.36±0.13	D
$12_{3,10} - 11_{3,9}$	41458.231±0.000			≤0.63	A,E
$13_{1,13} - 12_{1,12}$	41682.937±0.000			≤0.50	F
$13_{0,13} - 12_{0,12}$	41894.767±0.000			≤0.75	B
$12_{3,9} - 11_{3,8}$	42028.838±0.020	0.24±0.11	0.41±0.19	0.54±0.14	F
$12_{1,11} - 11_{1,10}$	42029.496±0.020	0.54±0.08	0.61±0.11	0.82±0.13	
$12_{2,10} - 11_{2,9}$	43009.536±0.015	0.40±0.12	0.49±0.19	0.76±0.20	A
$13_{2,12} - 12_{2,11}$	43930.042±0.000			≤0.54	
$14_{1,14} - 13_{1,13}$	44806.950±0.010	0.54±0.11	0.63±0.12	0.81±0.18	
$13_{3,11} - 12_{3,10}$	44904.123±0.030	0.71±0.13	1.26±0.24	0.53±0.16	G
$14_{0,14} - 13_{0,13}$	44964.612±0.015	0.20±0.07	0.42±0.15	0.45±0.16	
$13_{1,12} - 12_{1,11}$	45255.582±0.015	1.00±0.18	1.24±0.26	0.76±0.17	B
$13_{3,10} - 12_{3,9}$	45716.707±0.000			≤0.60	
$13_{2,11} - 12_{2,10}$	46628.461±0.000			≤0.75	H,B
$14_{2,13} - 13_{2,12}$	47187.614±0.000			≤0.54	
$15_{1,15} - 14_{1,14}$	47924.500±0.020	0.47±0.09	0.60±0.13	0.73±0.21	
$15_{0,15} - 14_{0,14}$	48039.847±0.020	0.58±0.12	0.94±0.16	0.58±0.22	
$14_{3,12} - 13_{3,11}$	48336.806±0.000			≤0.90	
$14_{1,13} - 13_{1,12}$	48420.601±0.020	0.46±0.17	0.83±0.25	0.52±0.28	I,B
$14_{3,11} - 13_{3,10}$	49443.118±0.000			≤1.0	

Notes. ^{a}Observed frequencies adopting a v_{LSR} of 5.83 km s^{-1} for TMC-1. ^{b}Integrated line intensity in mK km s^{-1}. ^{c}Linewidth at half intensity derived by fitting a Gaussian line profile to the observed transitions (in km s^{-1}). ^{A}Frequency switching data with a 10 MHz throw only. Negative feature present in the data with an 8 MHz throw. ^{B}Frequency switching data with an 8 MHz throw only. Negative feature present in the data with a 10 MHz throw. ^{C}Blended exactly at the same frequency with a line of H_2C_4N that contributes up to 60% of the observed feature. Assuming the remaining intensity is produced by this transition of fulvenallene, then the frequency of the transition may be 39354.949±0.030 MHz. ^{D}Blended with another feature. Fit still possible. ^{E}Upper limits correspond to three times the rms of the data. In these cases, frequencies correspond to those calculated with the recommended constants of Table 1. ^{F}Negative feature in both frequency switching data sets. ^{G}Line too broad. Probably blended with another feature. ^{H}Blended with a strong U feature. Unreliable fit. ^{I}Marginal detection.

Table C.2. Observed and calculated frequencies of c-$C_5H_4CCH_2$

Transition	ν^a_{obs} (MHz)	$\Delta\nu^b_{obs}$ (MHz)	ν^c_{cal} (MHz)	$\Delta\nu^d_{cal}$ (MHz)	$\nu_{obs}-\nu^e_{cal}$ (MHz)	Ref
$2_{1,2}$- $1_{1,1}$	6533.9975	0.0020	6533.9997	0.0004	−0.0022	1
$2_{0,2}$- $1_{0,1}$	6858.3532	0.0020	6858.3531	0.0002	0.0001	1
$2_{1,1}$- $1_{1,0}$	7209.1178	0.0020	7209.1148	0.0004	0.0030	1
$3_{1,3}$- $2_{1,2}$	9792.8921	0.0020	9792.8930	0.0006	−0.0009	1
$3_{0,3}$- $2_{0,2}$	10254.6211	0.0020	10254.6211	0.0004	0.0000	1
$3_{2,2}$- $2_{2,1}$	10307.2815	0.0020	10307.2792	0.0003	0.0023	1
$3_{2,1}$- $2_{2,0}$	10360.0099	0.0020	10360.0094	0.0004	0.0005	1
$3_{1,2}$- $2_{1,1}$	10805.2427	0.0020	10805.2412	0.0006	0.0015	1
$4_{1,4}$- $3_{1,3}$	13042.5047	0.0020	13042.5048	0.0007	−0.0001	1
$4_{0,4}$- $3_{0,3}$	13612.1720	0.0020	13612.1735	0.0005	−0.0015	1
$4_{2,3}$- $3_{2,2}$	13732.7538	0.0020	13732.7509	0.0004	0.0029	1
$4_{3,2}$- $3_{3,1}$	13768.4019	0.0020	13768.4014	0.0005	0.0005	1
$4_{3,1}$- $3_{3,0}$	13770.3390	0.0020	13770.3417	0.0005	−0.0027	1
$4_{2,2}$- $3_{2,1}$	13863.7014	0.0020	13863.7012	0.0006	0.0002	1
$4_{1,3}$- $3_{1,2}$	14390.7930	0.0020	14390.7923	0.0007	0.0007	1
$5_{1,5}$- $4_{1,4}$	16280.4664	0.0020	16280.4654	0.0009	0.0010	1
$5_{0,5}$- $4_{0,4}$	16920.4988	0.0020	16920.5009	0.0007	−0.0021	1
$5_{2,4}$- $4_{2,3}$	17149.4248	0.0020	17149.4194	0.0005	0.0054	1
$5_{3,3}$- $4_{3,2}$	17220.7569	0.0020	17220.7543	0.0006	0.0026	1
$5_{3,2}$- $4_{3,1}$	17227.5324	0.0020	17227.5312	0.0006	0.0012	1
$5_{2,3}$- $4_{2,2}$	17407.7712	0.0020	17407.7712	0.0009	0.0000	1
$5_{1,4}$- $4_{1,3}$	17961.4705	0.0020	17961.4710	0.0008	−0.0005	1
$6_{1,6}$- $5_{1,5}$	19504.9824	0.0020	19504.9813	0.0010	0.0011	1
$6_{0,6}$- $5_{0,5}$	20172.9326	0.0020	20172.9377	0.0011	−0.0051	1
$6_{2,5}$- $5_{2,4}$	20555.1800	0.0500	20555.1215	0.0005	0.0586	2
$6_{5,1}$- $5_{5,0}$	20646.8700	0.0500	20646.8382	0.0020	0.0318	2
$6_{5,2}$- $5_{5,1}$	20646.8700	0.0500	20646.8370	0.0020	0.0330	2
$6_{3,4}$- $5_{3,3}$	20678.2900	0.0500	20678.2760	0.0007	0.0140	2
$6_{3,3}$- $5_{3,2}$	20696.3100	0.0500	20696.2793	0.0008	0.0307	2
$6_{2,4}$- $5_{2,3}$	20996.5800	0.0500	20996.6225	0.0013	−0.0425	2
$6_{1,5}$- $5_{1,4}$	21512.3113	0.0020	21512.3128	0.0009	−0.0015	1
$7_{1,7}$- $6_{1,6}$	22714.9500	0.0500	22714.9139	0.0011	0.0361	2
$7_{0,7}$- $6_{0,6}$	23368.6900	0.0500	23368.6772	0.0015	0.0128	2
$7_{2,6}$- $6_{2,5}$	23947.7600	0.0500	23947.7488	0.0006	0.0112	2
$7_{6,1}$- $6_{6,0}$	24085.9100	0.0500	24085.9553	0.0034	−0.0453	2
$7_{6,2}$- $6_{6,1}$	24085.9100	0.0500	24085.9553	0.0034	−0.0453	2
$7_{5,3}$- $6_{5,2}$	24096.3600	0.0500	24096.3213	0.0022	0.0388	2
$7_{5,2}$- $6_{5,1}$	24096.3600	0.0500	24096.3279	0.0022	0.0321	2
$7_{3,5}$- $6_{3,4}$	24140.5000	0.0500	24140.4484	0.0009	0.0516	2
$7_{3,4}$- $6_{3,3}$	24180.7300	0.0500	24180.7009	0.0010	0.0291	2
$7_{2,5}$- $6_{2,4}$	24628.6800	0.0500	24628.7239	0.0019	−0.0439	2
$7_{1,6}$- $6_{1,5}$	25037.5386	0.0020	25037.5424	0.0010	−0.0038	1
$8_{1,8}$- $7_{1,7}$	25909.8500	0.0500	25909.8088	0.0013	0.0412	2
$8_{0,8}$- $7_{0,7}$	26513.6500	0.0500	26513.6530	0.0018	−0.0030	2
$8_{2,7}$- $7_{2,6}$	27325.3300	0.0500	27325.2866	0.0009	0.0434	2
$8_{7,2}$- $7_{7,1}$	27525.0300	0.0500	27524.9845	0.0054	0.0455	2
$8_{7,1}$- $7_{7,0}$	27525.0300	0.0500	27524.9845	0.0054	0.0455	2
$8_{6,2}$- $7_{6,1}$	27534.3500	0.0500	27534.3463	0.0038	0.0037	2
$8_{6,3}$- $7_{6,2}$	27534.3500	0.0500	27534.3461	0.0038	0.0039	2
$8_{5,3}$- $7_{5,2}$	27549.6600	0.0500	27549.6856	0.0025	−0.0256	2
$8_{5,4}$- $7_{5,3}$	27549.6600	0.0500	27549.6590	0.0025	0.0010	2

Table C.2. Continued

Transition	ν^a_{obs} (MHz)	$\Delta\nu^b_{obs}$ (MHz)	ν^c_{cal} (MHz)	$\Delta\nu^d_{cal}$ (MHz)	$\nu_{obs} - \nu^e_{cal}$ (MHz)	Ref
$8_{3,6}$- $7_{3,5}$	27606.0400	0.0500	27606.0689	0.0012	−0.0289	2
$8_{2,6}$- $7_{2,5}$	28295.7200	0.0500	28295.6725	0.0026	0.0475	2
$8_{1,7}$- $7_{1,6}$	28530.5400	0.0500	28530.5023	0.0014	0.0377	2
$9_{1,9}$- $8_{1,8}$	29089.9000	0.0500	29089.8668	0.0016	0.0332	2
$9_{0,9}$- $8_{0,8}$	29619.2800	0.0500	29619.2698	0.0022	0.0102	2
$9_{2,8}$- $8_{2,7}$	30685.8700	0.0500	30685.8656	0.0012	0.0044	2
$9_{8,1}$- $8_{8,0}$	30963.7400	0.0500	30963.8251	0.0080	−0.0851	2
$9_{8,2}$- $8_{8,1}$	30963.7400	0.0500	30963.8251	0.0080	−0.0851	2
$9_{7,3}$- $8_{7,2}$	30972.6200	0.0500	30972.6010	0.0060	0.0100	2
$9_{7,2}$- $8_{7,1}$	30972.6200	0.0500	30972.6010	0.0060	0.0100	2
$9_{6,4}$- $8_{6,3}$	30985.7800	0.0500	30985.7573	0.0043	0.0227	2
$9_{6,3}$- $8_{6,2}$	30985.7800	0.0500	30985.7581	0.0043	0.0219	2
$9_{3,7}$- $8_{3,6}$	31073.2100	0.0500	31073.2809	0.0016	−0.0709	2
$9_{3,6}$- $8_{3,5}$	31217.3080	0.0200	31217.3077	0.0022	0.0003	3
$9_{3,6}$- $8_{3,5}$	31217.2000	0.0500	31217.3077	0.0022	−0.1077	2
$9_{2,7}$- $8_{2,6}$	31983.3580	0.0150	31983.3859	0.0033	−0.0279	3
$9_{1,8}$- $8_{1,7}$	31983.7390	0.0100	31983.7384	0.0019	0.0007	3
$10_{1,10}$- $9_{1,9}$	32255.8540	0.0100	32255.8600	0.0020	−0.0060	3
$10_{0,10}$- $9_{0,9}$	32699.2590	0.0150	32699.2546	0.0024	0.0044	3
$10_{0,10}$- $9_{0,9}$	32699.2400	0.0500	32699.2546	0.0024	−0.0146	2
$10_{2,9}$- $9_{2,8}$	34027.8320	0.0150	34027.8258	0.0016	0.0063	3
$10_{2,9}$- $9_{2,8}$	34027.8100	0.0500	34027.8258	0.0016	−0.0158	2
$10_{9,1}$- $9_{9,0}$	34402.4400	0.0500	34402.4085	0.0114	0.0315	2
$10_{9,2}$- $9_{9,1}$	34402.4400	0.0500	34402.4085	0.0114	0.0315	2
$10_{8,3}$- $9_{8,2}$	34410.8900	0.0500	34410.8676	0.0088	0.0224	2
$10_{8,2}$- $9_{8,1}$	34410.8900	0.0500	34410.8676	0.0088	0.0224	2
$10_{7,3}$- $9_{7,2}$	34422.6900	0.0500	34422.7097	0.0066	−0.0197	2
$10_{7,4}$- $9_{7,3}$	34422.6900	0.0500	34422.7097	0.0066	−0.0197	2
$10_{6,4}$- $9_{6,3}$	34440.6000	0.0500	34440.5737	0.0048	0.0263	2
$10_{6,5}$- $9_{6,4}$	34440.6000	0.0500	34440.5709	0.0048	0.0292	2
$10_{4,7}$- $9_{4,6}$	34520.9400	0.0500	34520.9831	0.0026	−0.0431	2
$10_{4,6}$- $9_{4,5}$	34532.0500	0.0500	34532.0806	0.0026	−0.0306	2
$10_{3,8}$- $9_{3,7}$	34539.6790	0.0100	34539.6611	0.0023	0.0179	3
$10_{3,8}$- $9_{3,7}$	34539.6900	0.0500	34539.6611	0.0023	0.0289	2
$10_{3,7}$- $9_{3,6}$	34781.4170	0.0100	34781.4410	0.0033	−0.0240	3
$10_{3,7}$- $9_{3,6}$	34781.4500	0.0500	34781.4410	0.0033	0.0090	2
$10_{1,9}$- $9_{1,8}$	35389.3660	0.0100	35389.3691	0.0026	−0.0031	3
$10_{1,9}$- $9_{1,8}$	35389.4100	0.0500	35389.3691	0.0026	0.0409	2
$11_{1,11}$-$10_{1,10}$	35409.0190	0.0100	35409.0038	0.0025	0.0152	3
$11_{1,11}$-$10_{1,10}$	35409.0300	0.0500	35409.0038	0.0025	0.0262	2
$10_{2,8}$- $9_{2,7}$	35675.1550	0.0150	35675.1534	0.0042	0.0016	3
$10_{2,8}$- $9_{2,7}$	35675.1200	0.0500	35675.1534	0.0042	−0.0334	2
$11_{0,11}$-$10_{0,10}$	35766.1920	0.0150	35766.2148	0.0028	−0.0228	3
$11_{0,11}$-$10_{0,10}$	35766.1700	0.0500	35766.2148	0.0028	−0.0448	2

Table C.2. Continued

Transition	ν^a_{obs} (MHz)	$\Delta\nu^b_{obs}$ (MHz)	ν^c_{cal} (MHz)	$\Delta\nu^d_{cal}$ (MHz)	$\nu_{obs}-\nu^e_{cal}$ (MHz)	Ref
$11_{2,10}$-$10_{2,9}$	37349.8080	0.0150	37349.7879	0.0022	0.0201	3
$11_{2,10}$-$10_{2,9}$	37349.7700	0.0500	37349.7879	0.0022	−0.0179	2
$11_{10,1}$-$10_{10,0}$	37840.6200	0.0500	37840.6800	0.0156	−0.0600	2
$11_{10,2}$-$10_{10,1}$	37840.6200	0.0500	37840.6800	0.0156	−0.0600	2
$11_{9,3}$-$10_{9,2}$	37848.9500	0.0500	37848.9767	0.0124	−0.0267	2
$11_{9,2}$-$10_{8,1}$	37848.9500	0.0500	37848.9767	0.0124	−0.0267	2
$11_{8,3}$-$10_{8,2}$	37860.0100	0.0500	37860.0017	0.0097	0.0083	2
$11_{8,4}$-$10_{8,3}$	37860.0100	0.0500	37860.0017	0.0097	0.0083	2
$11_{7,4}$-$10_{7,3}$	37875.5500	0.0500	37875.5615	0.0073	−0.0115	2
$11_{7,5}$-$10_{7,4}$	37875.5500	0.0500	37875.5614	0.0073	−0.0114	2
$11_{6,5}$-$10_{6,4}$	37899.1900	0.0500	37899.1807	0.0054	0.0093	2
$11_{6,6}$-$10_{6,5}$	37899.1900	0.0500	37899.1717	0.0054	0.0183	2
$11_{3,9}$-$10_{3,8}$	38002.3630	0.0200	38002.3561	0.0031	0.0069	3
$11_{4,7}$-$10_{4,6}$	38024.7700	0.0500	38024.8792	0.0035	−0.1092	2
$11_{3,8}$-$10_{3,7}$	38383.9030	0.0200	38383.9494	0.0048	−0.0464	3
$11_{3,8}$-$10_{3,7}$	38383.9600	0.0500	38383.9494	0.0048	0.0106	2
$12_{1,12}$-$11_{1,11}$	38550.7840	0.0150	38550.8045	0.0034	−0.0205	3
$11_{1,10}$-$10_{1,9}$	38739.8860	0.0100	38739.8829	0.0035	0.0031	3
$11_{1,10}$-$10_{1,9}$	38739.8600	0.0500	38739.8829	0.0035	−0.0229	2
$12_{0,12}$-$11_{0,11}$	38829.5150	0.0150	38829.4924	0.0035	0.0226	3
$11_{2,9}$-$10_{2,8}$	39354.9490	0.0300	39354.9605	0.0053	−0.0115	3
$12_{2,11}$-$11_{2,10}$	40650.7430	0.0200	40650.7284	0.0028	0.0146	3
$12_{3,9}$-$11_{3,8}$	42028.8380	0.0200	42028.8560	0.0067	−0.0180	3
$12_{1,11}$-$11_{1,10}$	42029.4960	0.0200	42029.4421	0.0044	0.0539	3
$12_{2,10}$-$11_{2,9}$	43009.5360	0.0150	43009.5066	0.0065	0.0294	3
$14_{1,14}$-$13_{1,13}$	44806.9500	0.0100	44806.9533	0.0059	−0.0033	3
$13_{3,11}$-$12_{3,10}$	44904.1230	0.0300	44904.1187	0.0052	0.0043	3
$14_{0,14}$-$13_{0,13}$	44964.6120	0.0150	44964.6223	0.0058	−0.0103	3
$13_{1,12}$-$12_{1,11}$	45255.5820	0.0150	45255.5507	0.0053	0.0313	3
$15_{1,15}$-$14_{1,14}$	47924.5000	0.0200	47924.4911	0.0076	0.0089	3
$15_{0,15}$-$14_{0,14}$	48039.8470	0.0200	48039.8698	0.0075	−0.0228	3
$14_{1,13}$-$13_{1,12}$	48420.6010	0.0200	48420.5784	0.0063	0.0227	3

Notes. [a]Observed frequencies. [b]Uncertainty of the observed frequeciencies (MHz). [c]Calculated frequencies resulting from the fit (MHz). [d]Predicted uncertainty of the calculated frequencies (MHz). [e]Observed minus calculated frequencies (MHz). [1]Laboratoraty data from McCarthy et al. (2020). [2]Laboratory data from Sakaizumi et al. (1993) [3]This work.